A Domain Wall Model for Hysteresis in Ferroelastic Materials

Jordan E. Massad[1] **and Ralph C. Smith**[2]
Department of Mathematics
Center for Research in Scientific Computation
North Carolina State University
Raleigh, NC 27695-8205

Abstract

We develop a model that quantifies constitutive nonlinearities and hysteresis inherent to ferroelastic compounds, with emphasis placed on shape memory alloys. We formulate the model in two steps. First, we use the Landau theory of phase transitions to characterize the effective Gibbs free energy for both single-crystal and polycrystalline ferroelastics. The resulting nonlinear equations model equilibrium material behavior in the absence of impurities. Second, we incorporate pinning losses to account for the energy required to move domain walls across material inclusions. The full model is analogous to those developed by Jiles and Atherton for ferromagnetic compounds and Smith and Hom for ferroelectric materials. We illustrate aspects of the model through numerical simulations and comparisons with experimental stress-strain data.

Keywords: Ferroelastic hysteresis; shape memory alloy; domain wall theory; ferroelastic domain; superelasticity; Landau theory of phase transitions;anyhysteretic strain; domain wall pinning; pinning sites.

---

[1] Corresponding author; Email: jemassad@unity.ncsu.edu; Telephone: 919-515-3745; Fax: 919-515-1636.
[2] Email: rsmith@unity.ncsu.edu; Telephone: 919-515-7552.

# Report Documentation Page	*Form Approved* *OMB No. 0704-0188*

Public reporting burden for the collection of information is estimated to average 1 hour per response, including the time for reviewing instructions, searching existing data sources, gathering and maintaining the data needed, and completing and reviewing the collection of information. Send comments regarding this burden estimate or any other aspect of this collection of information, including suggestions for reducing this burden, to Washington Headquarters Services, Directorate for Information Operations and Reports, 1215 Jefferson Davis Highway, Suite 1204, Arlington VA 22202-4302. Respondents should be aware that notwithstanding any other provision of law, no person shall be subject to a penalty for failing to comply with a collection of information if it does not display a currently valid OMB control number.

1. REPORT DATE **2002**	2. REPORT TYPE	3. DATES COVERED **00-00-2002 to 00-00-2002**

4. TITLE AND SUBTITLE **A Domain Wall Model for Hysteresis in Ferroelastic Materials**	5a. CONTRACT NUMBER
	5b. GRANT NUMBER
	5c. PROGRAM ELEMENT NUMBER
6. AUTHOR(S)	5d. PROJECT NUMBER
	5e. TASK NUMBER
	5f. WORK UNIT NUMBER
7. PERFORMING ORGANIZATION NAME(S) AND ADDRESS(ES) **North Carolina State University,Center for Research in Scientific Computation,Raleigh,NC,27695-8205**	8. PERFORMING ORGANIZATION REPORT NUMBER
9. SPONSORING/MONITORING AGENCY NAME(S) AND ADDRESS(ES)	10. SPONSOR/MONITOR’S ACRONYM(S)
	11. SPONSOR/MONITOR’S REPORT NUMBER(S)

12. DISTRIBUTION/AVAILABILITY STATEMENT

Approved for public release; distribution unlimited

13. SUPPLEMENTARY NOTES

14. ABSTRACT

see report

15. SUBJECT TERMS

16. SECURITY CLASSIFICATION OF:			17. LIMITATION OF ABSTRACT	18. NUMBER OF PAGES **26**	19a. NAME OF RESPONSIBLE PERSON
a. REPORT **unclassified**	b. ABSTRACT **unclassified**	c. THIS PAGE **unclassified**			

Standard Form 298 (Rev. 8-98)
Prescribed by ANSI Std Z39-18

1 Introduction

A distinguishing feature of ferroelastic materials is the presence of hysteresis in the stress-strain relation. In shape memory alloys (SMAs), elastic hysteresis enables the materials to achieve very high work densities, produce large recoverable deformations, and generate high stresses, which are ideal for a number of current high performance applications. For example, medical and potential aeronautic and aerospace applications are being investigated to employ SMAs' large deformation and large force capabilities [14, 31]. Additionally, SMAs exhibit a damping capacity much larger than that of a number of conventional materials. In this case, SMA hysteresis is being utilized to design earthquake and hurricane-proof civil structures [13, 50, 62, 70].

In general, the material behavior of SMAs and other ferroelastics is nonlinear, hysteretic, and temperature dependent. To achieve the full potential of actuators using these materials, it is necessary to develop models that characterize the nonlinearities and hysteresis and to develop control algorithms based on those models. We propose a model that quantifies nonlinear material behavior in ferroelastic compounds, with emphasis placed on shape memory alloys. The physics-based model operates on a simplified domain representation of the material and lends itself to fast inversion for subsequent control design.

1.1 Ferroelastics and Shape Memory Alloys

A ferroelastic is a material in which there is a mechanical switching between orientation states of its underlying crystal structure. The switching process, called a ferroelastic phase transition, is a displacive structural phase transition that gives rise to an observable shape-change in the material. A measure of the crystal distortion is the *spontaneous strain*, analogous to the spontaneous magnetization and polarization associated with ferromagnetic and ferroelectric transitions, respectively. Measurements of spontaneous strains during ferroelastic phase transitions show ferroelastic material behavior to be generally nonlinear, exhibiting temperature-dependent elastic hysteresis (e.g., see [51]).

Shape memory alloys are a distinguishable class of ferroelastics that recover from up to 10% deformations via stress and temperature-induced phase transformations. SMAs undergo *martensitic transformations*, which are displacive transformations dominated by shear distortions of the crystal lattice. Transformations occur between two solid phases, called *martensite* and *austenite*, each distinguished by different crystallographic configurations. The martensitic transformations enable SMAs to recover or "remember" shape by two different mechanisms. First, the *shape memory effect* describes the phenomenon where the original shape of a plastically deformed sample is restored by heating. Upon heating deformed martensite, it transforms into austenite and correspondingly the SMA recovers its shape. Second, SMAs exhibit *superelasticity* at temperatures where austenite is a stable phase under no loading. In this case, austenite transforms into martensite due to an applied load. Upon unloading, the material reverts to austenite and correspondingly the SMA returns to its original geometry. As illustrated in Figure 1, there is hysteresis associated with these stress-induced phase transitions. Upon loading an austenite SMA, it behaves elastically until a loading transition point is reached. Loading beyond this point induces a transformation to the martensite phase with a large spontaneous strain. Upon unloading martensite, the crystal transforms back to austenite exhibiting zero strain (shape recovery). We refer the reader to [22] for details of the shape memory mechanisms and other SMA material properties.

At the heart of the first-order martensitic phase transitions in SMAs are displacive phase transitions in the crystal structure. NiTi and many Cu-based SMAs admit a cubic crystal structure (B2) in the high-temperature austenite phase. Upon transformation, the high-symmetry B2 structure

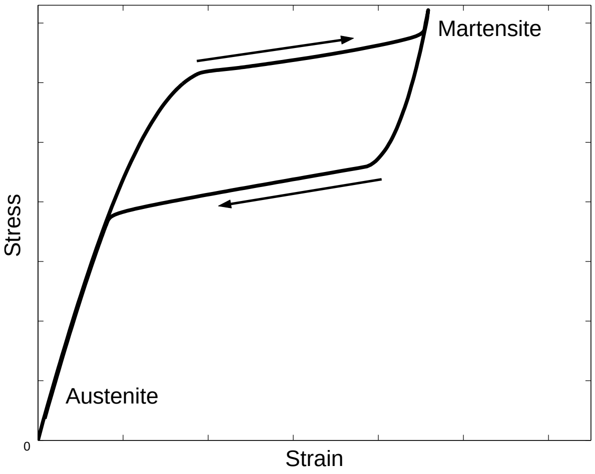

Figure 1: Idealized superelastic response of SMAs under uniaxial loading.

breaks down into lower-symmetry monoclinic (B19') martensite variants. Specifically in NiTi, the transformation corresponds to a reduction in space group symmetry from P$m3m$ to P$2_1/m$, and a single cubic austenite crystal transforms into one of 24 martensite variants. The transformation is nearly volume preserving (∼0.5% change) corresponding to predominantly shear deformations on the order of 10% across crystal habit planes [25]. Considering deformations along one axis (across a single habit plane), an SMA crystal admits either the austenite (A) phase or one of two martensite variants ($M^{\pm}$). In this simple case, $M^{\pm}$ are sheared versions of A, as illustrated in Figure 2.

SMAs can be prepared as a single crystal, but they occur more naturally as polycrystalline compounds. A *single-crystal* SMA refers to a homogeneous, isotropic SMA specimen that consists of unit cells of only one crystallographic orientation. A *polycrystalline* SMA consists of many single-crystal domains with different orientations. The behavior of single-crystal SMAs differs from that of polycrystalline SMAs in several aspects. For instance, single-crystal NiTi recovers from up to 10% tensile strains, depending on the crystal orientation, while polycrystalline NiTi typically recovers no more than 8% tensile strains [5]. We model aspects of both single-crystal and polycrystalline SMAs using a homogenization technique based on a description of moving ferroelastic domain walls.

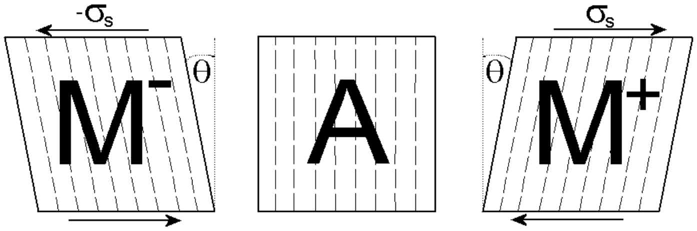

Figure 2: A single crystal under uniaxial loading admits three stable configurations: austenite (A) and martensite variants ($M^{\pm}$). The arrows indicate shearing and the associated shear strain is $\varepsilon_s = \tan\theta$.

1.2 Ferroelastic Domains

Ferroelastic *domains* are regions of ferroelastic crystals distinguished by different strain states of definite crystallographic orientation [51, 64]. Roytburd, who originally formulated the more general concept of *elastic domains*, shows that domains form in ferroelastics to minimize internal elastic energies [49]. Accordingly, ferroelastic domains in SMAs correspond to stable martensite and austenite strain states. Ferroelastic *domain walls* are boundaries or transition regions where strains change gradually between adjacent domains. In fact, phase transformations in SMAs proceed with the motion of domain walls as discussed in [17, 52]. When a transformation occurs, domains exhibit spontaneous strains and their corresponding domain walls *translate*. In addition to translating, domain walls can *bend* about *pinning sites*, which characterize material impurities, inclusions, or inhomogeneities that hinder domain wall movement [37, 52].

It is commonly accepted that domain wall motion in ferroelastic materials yield hysteretic macroscopic behavior. Mueller, et. al. indicate in [41] that nonlinear effects in ferroelastic crystals are related to the properties of ferroelastic domain walls pinned on defects, which de-pin above some stress level. Additionally, Jian and Wayman [32] observe domain wall motion in single-crystal and polycrystalline $LaNbO_4$ ferroelastics under stress and argue that the nonlinear elastic material behavior and the observed shape memory effect are the result of domain wall motion. They also reason that polycrystalline grain boundaries, like pinning sites, limit wall mobility. Furthermore, Newnham [43] concludes that stress-induced movement of domain walls is a source of the hysteresis observed in ferroelastics, and Salje [51] claims that macroscopic spontaneous strains resulting from martensitic transformations are strongly influenced by a crystal's domain structure.

Many have established an analogy between ferroelastic domains and their ferromagnetic and ferroelectric counterparts [7, 12, 16, 32, 41, 43, 48, 49, 57, 66]. In particular, Prieb, et. al. remark on the similarities between ferroelastic and ferromagnetic hysteresis data and suggest that the similarities arise from common domain rearrangement mechanisms resulting from exogenous fields. They propose that ferroelastic hysteresis is caused by the pinning of phase boundaries on lattice defects, as ferromagnetic hysteresis can be caused by the pinning of ferromagnetic domain walls. Furthermore, like Salje [51], they identify a ferroelastic coercive stress analogous to the coercive fields in ferromagnetic and ferroelectric hysteresis. However, as discussed in [28], ferroelastic domain walls are typically an order of magnitude thicker than ferromagnetic domain walls, so as in ferroelectrics, reversible wall effects in ferroelastics are expected to be more substantial.

Given the experimental results of [32, 48] and the strong comparisons to ferromagnetic and ferroelectric domain theory, a ferroelastic domain theory may provide a viable means for describing the nonlinear constituent behavior of SMAs. In the next section, we summarize common approaches for modeling hysteresis in ferroelastic materials. We also summarize a domain model methodology for ferromagnetics and ferroelectrics that we consider for ferroelastics.

1.3 Modeling Approaches

Most models of hysteresis in SMAs are constitutive, aiming to predict the measured relationships among stress, temperature, and strain. We refer the reader to reviews and comparisons of a number of models in [6, 10, 20, 25, 47] and particularly in [53], where computational considerations are addressed. Ferroelastic and SMA hysteresis models can be roughly categorized as being *microscopic*, *mesoscopic*, or *macroscopic*, depending on which material level they base their method of predicting constitutive behavior.

Microscopic and mesoscopic models such as [2, 3, 11, 71] employ both phenomenological and first-principles theories to model atomic and lattice-level behavior of ferroelastics. Understanding material dynamics at these fundamental levels can support efforts to design compounds with desired material properties. For example, Castán, et. al. [11] quantify interatomic energies and conduct lattice model simulations for some ferroelastic alloys. Given atomic composition and thermal treatment information, they are able to compute macroscopic elastic constants and martensite transition temperatures. Models of this nature are typically used for off-line simulations, and their solution requires techniques such as Monte Carlo methods that have a high computational cost.

Another class of mesoscopic models, traditionally referred to as *micromechanical* models, focuses specifically on developing local grain-level constitutive theories [18, 24, 45]. While operating at a fundamental level similar to that of the previously mentioned approaches, these models provide a more direct means of predicting observed constitutive behavior. Deriving macroscopic constitutive behavior from these theories for design applications necessitates additional procedures, such as the self-consistent averaging approaches in [24, 45]. Scaling these mesoscopic theories to macroscopic levels usually is computationally intensive; therefore, for macroscopic predictions, these models are generally not intended for on-line engineering nor control applications.

Macroscopic models commonly employ phenomenological or energy principles. As opposed to most microscopic and mesoscopic models, macroscopic models are formulated mainly for implementation into engineering designs and on-line control. A series of internal-state models rooted in the uniaxial Tanaka approach [6, 47] use an empirical or thermodynamics-based evolution law for the martensite volume fraction, which in-turn is used to predict stress or strain using a phenomenological constitutive relation. Similarly, Papenfuss and Seelecke [44] predict thermomechanical behavior by modeling the evolution of martensite variant fractions, but by using a statistical thermodynamics description of thermally activated processes.

Another macroscopic approach, based on phenomenological principles, is the Preisach model [68]. Originally developed for ferromagnetic hysteresis, Preisach models have been generalized and adapted to other physical systems, including SMAs [23, 29, 30, 35, 36, 40, 69]. In general, Preisach models are purely empirical and their implementation reduces to the identification of many mathematical parameters via numerous hysteresis experiments that may be unavailable in practice. To make Preisach models more tractable for SMA applications, there have been attempts to replace or identify purely mathematical constructs with known or approximated physics. For example, Huo [30] incorporates Falk's [15] macroscopic Landau-Ginzburg potential to account for first-order martensitic phase transformations. In addition, Lagoudas and Bhattacharyya [36] associate Preisach weighting functions with distributions of single-crystal orientations in polycrystalline SMAs.

The model we present focuses on predicting macroscopic constitutive behavior by considering mesoscopic (domain level) energy relations. We derive our model based on the Jiles-Atherton domain wall model formulation, first used to predict ferromagnetic hysteresis in [33] and subsequently ferroelectric hysteresis in [56]. Previous work to employ these techniques for ferroelastics includes [39, 66]. We take this approach for three main reasons. First, the Jiles-Atherton approach, leads to models with few parameters, most of which can be readily identified from measurements and all of which can be updated quickly. Second, the model formulation is of low-order and lends itself to control design; it has been implemented into control algorithms via inverse compensation [55]. Third, successful adaptation of the Jiles-Atherton framework to ferroelastics could provide a crucial step towards developing a unified methodology for modeling hysteresis in ferroic materials [57].

While many have investigated domain phenomena in ferroelastics, as described in the previous section, few have related domain wall theory to macroscopic hysteresis explicitly. In particular, Brokate and Sprekels [7] develop constitutive equations based on Falk's free energy formulation to predict temperature-dependent stress-strain hysteresis, but no comparison to data is provided. Likewise, Stoilov and Bhattacharyya [61] model SMA hysteresis by describing the evolution of phase fronts (domain walls) during transformation. Neither accounts for material defects nor treats minor loops.

In the following sections, we formulate the model in two steps. In the first, we develop nonlinear constitutive relations that characterize the stress-strain behavior of defect-free ferroelastic compounds in thermodynamic equilibrium. We achieve this by first considering the elastic energy for a single crystal and then by averaging over grains to obtain an effective energy for a polycrystal. The resulting nonlinear constitutive equations predict hysteresis in which phase transformations occur instantaneously and phase boundaries propagate unhindered. In the second step, we incorporate the effects of material inclusions and formulate the energy dissipated by the motion of phase boundaries across those inclusions. The resulting domain wall model predicts stress-strain hysteresis under quasi-static, isothermal conditions. Finally, we demonstrate the temperature dependent hysteresis predicted by the model via numerical simulations, we discuss model parameter identification from measurements, and we validate our model with superelastic SMA hysteresis data.

2 Nonlinear Stress-strain Law

In this section, we derive a stress-strain law to model the superelastic response of SMAs in thermodynamic equilibrium. Shape memory mechanisms in SMAs are caused by first-order martensitic phase transformations. Accordingly, by describing these structural phase transformations, we yield an expression for the stress-strain material response. Our approach follows from energy methods used in the nonlinear theory of finite thermoelasticity, where the construction of a multi-well strain-energy function is used to characterize constitutive behavior [1]. Free energy expressions for SMAs have been developed through various approaches [1, 4]. We take a phenomenological approach based on the *Landau theory of phase transitions*, which has been shown to yield appropriate approximations for the free energies corresponding to ferroelastic phase transitions [51] and has been used for SMA modeling in [7, 16, 19, 39, 51, 61, 66]. In addition to ferroelastics, the Landau theory has been successful in modeling transitions in ferroelectrics and ferromagnetics [15].

First, we summarize the Landau theory currently established for SMAs, and we quantify the free energy of a single crystal as a function of strain. Second, we adapt the single-crystal energy function to accommodate bulk polycrystalline specimens under tensile loading. Third, we obtain a stress-strain law from the effective free energy equations of state. Our ultimate result is a thermodynamic equilibrium relation predicting relative macroscopic elongation due to an applied stress at a fixed temperature.

2.1 The Landau Free Energy

The Landau theory is a phenomenological theory that establishes the consistency of microscopic crystal characteristics, such as space-symmetry, with macroscopic quantities, such as elasticity. Using lattice dynamics, elasticity theory, and group theory, it aims to derive a system free energy based on the symmetry changes of a crystallographic phase transformation. In constructing the free energy expression, the Landau theory defines two fundamental concepts: the *order parameter* and the *Landau free energy*.

The order parameter is a thermodynamic quantity of the system that distinguishes one phase from another. Identifying the order parameter for a particular phase transformation is nontrivial. In some cases, such as purely strain-induced ferroelastic transitions, the spontaneous strain characterizes the order parameter [64]. However, in general this is not the case, and the order parameter can be related to the softening of phonon modes or to an orientational ordering process, for example [2, 3, 46, 51, 65]. In the case of martensitic transformations exhibited by SMAs and similar ferroelastics, there has been controversy over the specification of the order parameter. Traditionally, spontaneous strain, which distinguishes austenite domains from martensite domains, is treated as the order parameter [15, 16, 19, 66]. However, recent studies have shown that martensitic phase transitions are *improper*, treating macroscopic transformation strain as a secondary effect coupled to the primary order parameter. The primary order parameter, which solely determines the symmetry-breaking mechanism, instead is expressed in terms of normal mode components of lattice modulation wave vectors [2, 3, 46]. In its group theoretical formulation, the Landau theory restricts the order parameter to a quantity that spans the irreducible representation driving the symmetry-breaking transition.

The Landau free energy is a thermodynamic expression determined by symmetry properties of the crystallographic phase transformation. It is in the form of a polynomial expansion whose terms are invariant functions under the symmetry operations of the high-symmetry space group. For general ferroelastics, the Landau free energy is a function of the order parameter and spontaneous strain

$$L\left(Q_i,\varepsilon_i\right) = L_Q\left(Q_i\right) + L_\varepsilon\left(\varepsilon_i\right) + L_{Q\varepsilon}\left(Q_i,\varepsilon_i\right), \tag{1}$$

where L_Q is the expansion of the order parameter components Q_i, L_ε is the elastic energy expressed in terms of spontaneous strain components ε_i (Voigt notation), and $L_{Q\varepsilon}$ is the order parameter-strain coupling energy. The analytical form of the expansions is dictated by the symmetry of the high-symmetry phase *and* the symmetry breaking that leads to the low-symmetry phase. The cubic-monoclinic transformation in NiTi corresponds to the symmetry breaking from group O_h to group C_{2h}. Group theoretic methods for constructing the Landau free energy in terms of multi-component OPs for all seven crystal systems are provided in [65], while analyses of the cubic-monoclinic transformations in NiTi and similar compounds are detailed in [3, 19, 63, 64]. For example, truncated to sixth-order, the order parameter expansion invariant with respect to the cubic symmetry group O_h is

$$L_Q\left(Q_i\right) = \frac{\beta_0}{2}I_1 + \frac{\beta_1}{4}I_2 + \frac{\beta_2}{4}I_1^2 + \frac{\beta_3}{6}I_1^3 + \frac{\beta_4}{6}I_1I_2 + \frac{\beta_5}{6}I_3^2, \tag{2}$$

where

$$I_1 = \left(Q_1^2 + Q_2^2 + Q_3^2\right),\ I_2 = \left(Q_1^4 + Q_2^4 + Q_3^4\right),\ I_3 = Q_1Q_2Q_3, \tag{3}$$

for a three-component order parameter. In general, the energy coefficients β_i are temperature-dependent. The standard assumption in the Landau theory is that only the coefficient of the quadratic term depends on temperature and that it is proportional to $(T - T_0)$, where T is the system temperature and T_0 is the critical temperature of the phase transition, analogous to the Curie temperature for ferroelectrics and ferromagnetics. This assumption, motivated by specific entropy and enthalpy considerations in [51], guarantees that the high-symmetry phase corresponds to a stable, stress-free *high-temperature* phase for $T > T_0$. Evidence for temperature-dependence in other coefficients is reported in [19, 67] for specific ferroic compounds. In (2), the Landau free energy accounts for transformations to and among four distinct low-symmetry phases. (An expansion to twelfth-order accounts for a maximum of eight phases.) By considering only those transformations and phases pertinent to the first-order B2-B19' transformation in NiTi, the form of (2) simplifies to

$$L_Q\left(Q\right) = \frac{b_2(T - T_0)}{2}Q^2 + \frac{b_4}{4}Q^4 + \frac{b_6}{6}Q^6, \tag{4}$$

where Q is a scalar order parameter, and the effective coefficients b_2, b_4, b_6, and temperature T_0 are combinations of coefficients for multi-component expansions. Simplification and reduction of general expansions is discussed in [51, 65]. We note that with $b_2, b_6 > 0$ and $b_4 < 0$, (4) is the minimum-order order parameter expansion that describes the first-order phase transition under the symmetry constraints. In the Landau theory, typically one uses the expansion of lowest-order to model a phase transition with as simple a model as possible.

The elastic and coupling energies are left to be defined. Using standard Voigt notation, we take the symmetry-obeying elastic energy expansion

$$L_\varepsilon\left(\varepsilon_i\right)=\frac{1}{2}\sum_{i,j=1}^{6}\left(c_{ij}\varepsilon_i\varepsilon_j\right)+\frac{1}{2}\sum_{i,j=1}^{6}\left(c_{ijkl}\varepsilon_i\varepsilon_j\varepsilon_k\varepsilon_l\right), \tag{5}$$

where c_{ij} and c_{ijkl} are second-order and fourth-order elastic coefficients, respectively. A thermodynamic description of high-order elastic coefficients is provided in [8], and [59, 60] describe methods for measuring those of single crystals. Symmetry of the Landau free energy restricts terms of the order parameter-strain coupling energy to linear combinations of $Q_i^n\varepsilon_i^m$, with integers $m > n > 0$. Conserving the symmetry of the improper phase transition we take a biquadratic coupling

$$L_{Q\varepsilon}\left(Q,\varepsilon_i\right)=\frac{1}{2}Q^2\sum_{i,j=1}^{6}d_{ij}\varepsilon_i\varepsilon_j \tag{6}$$

with a scalar order parameter and the constant coupling coefficients d_{ij}. Refer to [51] for details on other coupling scenarios and measurements of the coupling coefficients.

The P$m3m$ to P$2_1/m$ symmetry breaking in NiTi restricts the spontaneous strain tensor components to four nonzero shear strains [51]. For a one-dimensional model, we consider a single nonzero shear component ε_s, which yields

$$L_\varepsilon\left(\varepsilon_s\right)=\frac{c_{ss}}{2}\varepsilon_s^2+\frac{c_{ssss}}{4}\varepsilon_s^4$$

and

$$L_{Q\varepsilon}\left(Q,\varepsilon_s\right)=\frac{d_{ss}}{2}Q^2\varepsilon_s^2.$$

Therefore the reduced Landau free energy in one spatial dimension is

$$L\left(Q,\varepsilon_s\right)=\frac{b_2(T-T_0)}{2}Q^2+\frac{b_4}{4}Q^4+\frac{b_6}{6}Q^6+\frac{c_{ss}}{2}\varepsilon_s^2+\frac{c_{ssss}}{4}\varepsilon_s^4+\frac{d_{ss}}{2}Q^2\varepsilon_s^2. \tag{7}$$

Similar to techniques employed in [46, 51, 65, 66], we obtain a free-energy function solely in terms of strain by enforcing the stress-free equilibrium conditions

$$\frac{\partial L}{\partial Q}=0 \text{ and } \frac{\partial L}{\partial \varepsilon_s}=0,$$

which yields the relations

$$Q\left(b_2(T-T_0)+b_4Q^2+b_6Q^4+d_{ss}\varepsilon_s^2\right)=0 \tag{8}$$

$$\varepsilon_s\left(c_{ss}+c_{ssss}\varepsilon_s^2+d_{ss}Q^2\right)=0. \tag{9}$$

By construction, vanishing Q corresponds to the high-temperature/symmetry phase, which we associate with zero deformation (austenite). Therefore, taking $\varepsilon_s \neq 0$ in (9) yields

$$Q^2=-\frac{c_{ss}+c_{ssss}\varepsilon_s^2}{d_{ss}}.$$

Then (8) implies

$$\left[b_2\left(T-T_0\right)-\frac{b_4 c_{ss}}{d_{ss}}+\frac{b_6 c_{ss}^2}{d_{ss}^2}\right]+\left(d_{ss}-\frac{b_4 c_{ssss}}{d_{ss}}+2\frac{b_6 c_{ss} c_{ssss}}{d_{ss}^2}\right)\varepsilon_s^2+\frac{b_6 c_{ssss}^2}{d_{ss}^2}\varepsilon_s^4=0. \tag{10}$$

Scaled by a factor of ε_s, we take (10) as the equilibrium condition for an effective free energy in terms of shear strain

$$L_e\left(\varepsilon_s\right)=\frac{a_6^s}{6}\varepsilon_s^6-\frac{a_4^s}{4}\varepsilon_s^4+\frac{a_2^s}{2}\left(T-T_c\right)\varepsilon_s^2, \tag{11}$$

with effective parameters

$$T_c=T_0+\frac{c_{ss}\left(b_4 d_{ss}-b_6 c_{ss}\right)}{b_2 d_{ss}^2},\ a_2^s=b_2,\ a_4^s=\frac{c_{ssss}\left(b_4 d_{ss}-2b_6 c_{ss}\right)}{d_{ss}^2}-d_{ss},\ \text{and } a_6^s=\frac{b_6 c_{ssss}^2}{d_{ss}^2}.$$

By expressing the Landau free energy in terms of effective quantities, we have avoided assigning a physical definition to the order parameter at the risk of losing the ability to experimentally verify the expansion coefficients. Nevertheless, we can use experimental nonlinear elastic and coupling constants to validate orders of magnitude of least-squares fits to data. Provided $T_c, a_2^s, a_4^s, a_6^s > 0$, (11) maintains the overall equilibrium behavior established by symmetry in (4). Including higher-order nonlinear elastic terms in (5) results in an effective Landau free energy of higher-order. While a similar effect may be realized by increasing the order of the order parameter expansion, only the lowest-order expansion in (4) is necessary to guarantee a first-order transition to the monoclinic phase. As for the coupling energy, there lacks evidence that terms $Q^n\varepsilon_i^m$ for $m+n>4$ contribute significant amounts of energy in ferroelastics [51]. Based on these arguments, we use an extension to (11)

$$L_e^m\left(\varepsilon_s\right)=\sum_{j=3}^{m}\left(\frac{a_{2j}^s}{2j}\right)\varepsilon_s^{2j}-\frac{a_4^s}{4}\varepsilon_s^4+\frac{a_2^s}{2}\left(T-T_c\right)\varepsilon_s^2 \tag{12}$$

for $m \geq 3$ odd, which we take to reflect higher-order elastic nonlinearities in the material. For constants a_{2j}^s, we only restrict *a priori* $a_2^s, a_4^s, a_{2m}^s > 0$ to ensure the observed first-order transition at $T_c > 0$ and stability for large ε_s. In general, we determine the effective coefficients for a specific SMA or transducer through a least-squares fit to data. Note that (12) corresponds to the expansion of a scalar order parameter, invariant with respect to triclinic crystal symmetry with point group $\bar{1}$ [65].

In [16, 19], (11) is used to characterize uniaxial phase transformations in SMAs where T_c marks the temperature below which austenite is unstable. The free energy function has up to three minima; the energy minimum at $\varepsilon_s = 0$ corresponds to the high-temperature austenite phase, while the symmetric lateral minima correspond to the martensite variants as illustrated in Figure 3. The free-energy in (12) is a reference free energy with respect to the free energy of stress-free austenite, since it neglects other energy contributions. Those contributions, such as chemical free energy, depend solely on temperature, and thus are inconsequential to isothermal stress-strain behavior [51].

2.2 Effective Gibbs Free Energy

The Landau theory provides us with a free energy expression in terms of shear strain of a single crystal. The expression (12) is the reference Helmholtz free energy density at a fixed temperature T. Including the effects of an external field, we get the associated Gibbs free energy density

$$G_s\left(\varepsilon_s;\sigma_s\right)=\sum_{j=3}^{m}\left(\frac{a_{2j}^s}{2j}\right)\varepsilon_s^{2j}-\frac{a_4^s}{4}\varepsilon_s^4+\frac{a_2^s}{2}\left(T-T_c\right)\varepsilon_s^2-\sigma_s\varepsilon_s, \tag{13}$$

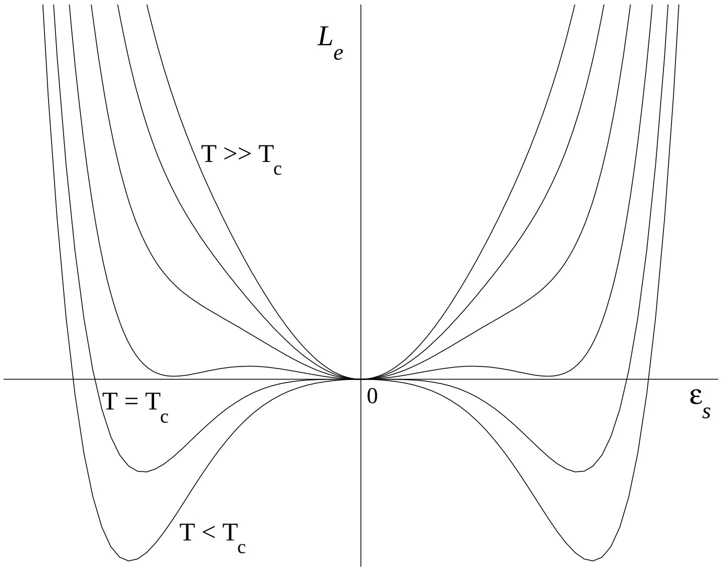

Figure 3: A Landau free energy (11) describing a crystallographic system with three equilibrium phases.

where σ_s is the shear stress conjugate to ε_s. We reformulate (13) in terms of tensile strains related to measured elongation and of tensile stresses (forces) applied to an SMA. The shear stress and strain of a uniaxially loaded element are related to tensile (normal) quantities as follows:

$$\sigma_s = \sigma \sin\phi \cos\phi \tag{14}$$

$$\varepsilon = \varepsilon_s \sin\phi \cos\phi, \tag{15}$$

where the element is oriented at an angle $\pi/2 - \phi$ with respect to the normal stress σ, and the measured engineering strain of the specimen is ε. Therefore, (13) has the form

$$G_\phi(\varepsilon;\sigma) = \sum_{j=3}^{m} \left(\frac{a_{2j}^{\phi}}{2j} \right) \varepsilon^{2j} - \frac{a_4^{\phi}}{4}\varepsilon^4 + \frac{a_2^{\phi}}{2}(T - T_c)\varepsilon^2 - \sigma\varepsilon, \tag{16}$$

where

$$a_{2j}^{\phi} = \left(\frac{2}{\sin(2\phi)} \right)^{2j} a_{2j}^{s}, \quad \phi \in \left(0, \frac{\pi}{2}\right). \tag{17}$$

In a stressed polycrystalline compound, each single-crystal region exhibits a different amount of crystallographic shear. In this case, there are many grains with different orientations ϕ. We get an effective, macroscopic free energy for a polycrystal, by integrating over single-crystal grain orientations [16].

$$\begin{aligned} G(\varepsilon;\sigma) &= \int_0^{\pi/2} G_\phi(\varepsilon;\sigma) f(\phi) d\phi \\ &= \sum_{j=3}^{m} \frac{a_{2j}}{2j}\varepsilon^{2j} - \frac{a_4}{4}\varepsilon^4 + \frac{a_2}{2}(T - T_c)\varepsilon^2 - \sigma\varepsilon, \end{aligned} \tag{18}$$

where

$$a_{2j} = \int_0^{\pi/2} a_{2j}^{\phi} f(\phi) d\phi. \tag{19}$$

Here, $f(\phi)$ represents a scaled statistical distribution of single-crystal orientations. The formulation of effective coefficients a_{2j} in (19) is well defined, despite the singularities in the integrands at $\phi = 0$ and $\pi/2$. At these orientations, the applied stress has no shear component. Since we assume that the proportion of grains that do not shear is negligible, we choose a distribution function $f(\phi)$ that removes the singularities. Ultimately, the macroscopic free energy (18) differs from (13) only in the scaling of its terms.

2.3 Stress-Strain Equations

We derive a stress-strain law from (18) by employing equilibrium principles. The equilibrium state of the material is the strain value that yields a minimum Gibbs free energy given a stress σ at fixed temperature T. The stable equilibrium states $(\varepsilon_{an}, \sigma, T)$ must satisfy the conditions

$$\left.\frac{\partial G}{\partial \varepsilon}\right|_{\varepsilon_{an},\sigma,T} = 0 \text{ and } \left.\frac{\partial^2 G}{\partial \varepsilon^2}\right|_{\varepsilon_{an},\sigma,T} > 0. \tag{20}$$

Evaluating the conditions yields

$$\sum_{j=3}^{m} a_{2j} \varepsilon_{an}^{2j-1} - a_4 \varepsilon_{an}^3 + a_2 (T - T_c) \varepsilon_{an} = \sigma \tag{21}$$

subject to

$$\sum_{j=3}^{m} (2j-1) a_{2j} \varepsilon_{an}^{2j-2} - 3a_4 \varepsilon_{an}^2 + a_2 (T - T_c) > 0, \tag{22}$$

where ε_{an} is the strain at equilibrium.

The stress-strain relationship (21) is nonlinear and multivalued, and its solution is path-dependent. For a sixth-order expansion, there are at most three solutions for a given stress; each strain corresponds to one of the three crystal phases. As shown in Figure 4, the stress-strain response is temperature-dependent and hysteretic. Note that the model predicts instantaneous phase transitions, corresponding to the discontinuities in the hysteresis loops. This behavior is a characteristic of the Landau theory of phase transitions, since it is assumed that a crystal can reach its equilibrium configurations instantaneously. Issues concerning the description of superelastic hysteresis via a Landau potential are discussed in [42]. In particular, the equilibrium behavior predicted in (21) describes the *maximum* hysteresis exhibited by a material. That is, the phase transformations are thermodynamically likely to occur at any point in the metastable regions of the stress-strain curves [16, 42]. Therefore, as is, the model predicts a stabilized hysteresis loop where a full transformation to martensite has occurred upon loading. In the next section, we incorporate phase boundary effects which prohibit discontinuous transitions (21).

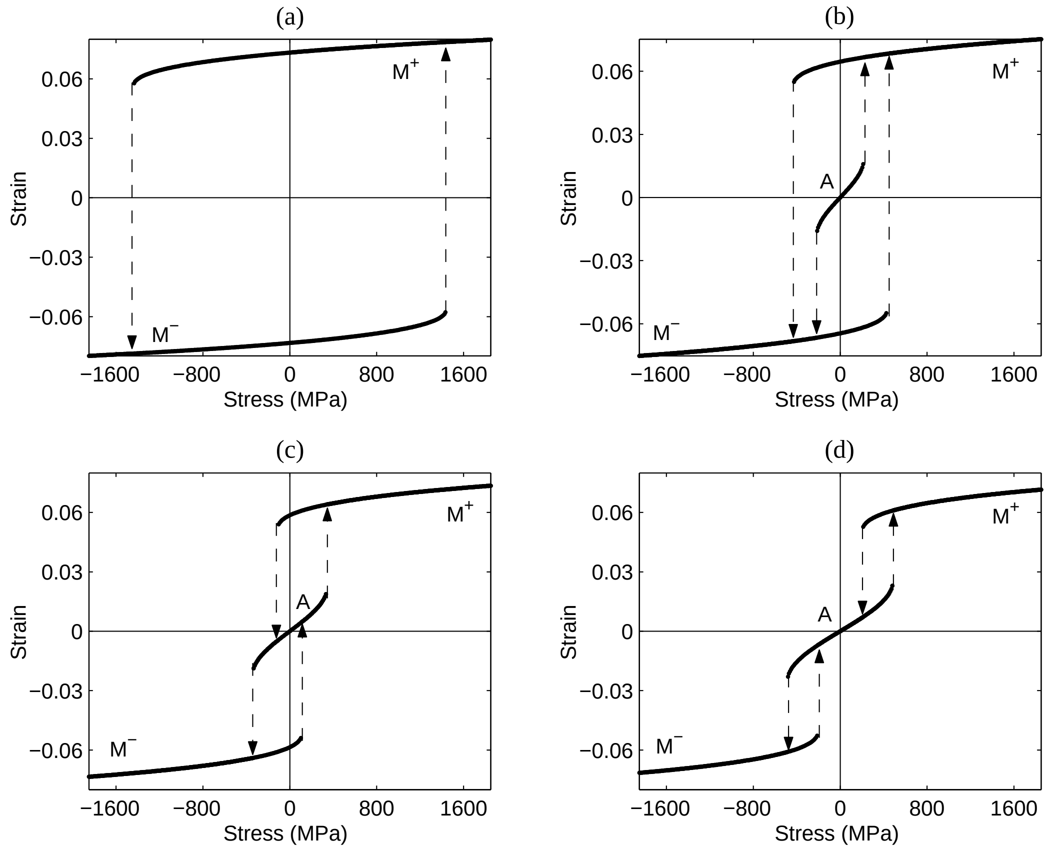

Figure 4: The equilibrium stress-strain model for increasing temperatures - from the quasiplastic regime $T < T_c$ (a) to the pseudoelastic (superelastic) regime (d). There are up to three equilibrium branches, corresponding to austenite and the martensite variants.

3 The Domain Wall Model

The Landau-based constitutive theory of lattice-level behavior suggests that a material responds discontinuously when brought across a transformation point. The thermodynamic equilibrium relation (21) derived from the Landau free energy also predicts discontinuous behavior at the macroscopic level, however, which is not an observed phenomenon [22, 54, 66]. Solutions to this dilemma have been to use a Landau-Ginzburg free energy to augment the Landau potential with strain-gradient terms. The result of this approach is an expression for the geometry and motion of phase boundaries as transverse shock waves in the absence of material dislocations [17, 61]. Realistically, ferroelastics contain material inclusions and other inhomogeneities that are manifest as an internal friction that inhibits phase boundary motion and that dissipates elastic energy. To account for impurities and energy losses, we treat the macroscopic measured strain ε as a result of crystal domain reorientations impeded by lattice defects. We call the strain that would be measured in the absence of material inhomogeneities the *anhysteretic strain*, ε_{an}. By definition, the anhysteretic quantity in the Jiles-Atherton framework represents the system response that would be obtained in the absence of hysteresis effects. In [33, 56, 58], each point on an anhysteretic curve corresponds to a global energy minimum for a given external field. Accordingly, this interpretation restricts the single-valued anhysteretic strain to lie on only the absolutely stable portions of the equilibrium strain curves illustrated in Figure 4. The absolutely stable states represent the Maxwell states of an elastic body [1, 16, 42]. As in [66], we interpret the anhysteretic strain in ferroelastics to be identical to the *multivalued* equilibrium strain in (21), which reflects both absolutely stable and metastable energy states.

In addition to ε_{an}, we identify two macroscopic strains that are brought about by domain wall motion. We denote the *irreversible strain* ε_{ir} as that which manifests from domain wall translation across pinning sites. We denote the *reversible strain* ε_{re} as that which manifests from domain wall bending about pinning sites. The total macroscopic strain ε is the sum of the two. In this section, we quantify irreversible and reversible strains in terms of ε_{an} to predict measured bulk strain.

3.1 Domain Wall Pinning

Pinning sites are typically due to material impurities, inclusions, or inhomogeneities that effectively hinder the natural motion of domain boundaries. In magnetic materials, Jiles and Atherton assume that pinning sites are uniformly distributed, localized entities with equal energy proportional to an average domain wall energy [33, 56, 58]. We make these assumptions in our analysis; however we distinguish three classes of domain walls for any single orientation corresponding to the boundaries among A, M^+, and M^- phases. Falk treats the motion of this class of domain walls in [17]. Under an increasing stress, phase transformations occur at the transformation stress $\sigma^{\beta}(T)$, where $\beta \in \{\mp, -A, A+\}$ denotes the switch from M^- to M^+, M^- to A, and A to M^+, respectively. The strain $\varepsilon_{\beta}^{tr}(T)$ is the spontaneous transformation strain accompanying the domain switching, illustrated by the jumps in Figure 4, which is essentially the strain manifested by wall translation. For an applied stress $\sigma \geq \sigma_{\beta}(T)$ at temperature T,

$$\mathcal{E}_{\beta}(T) = \int \sigma(\varepsilon)\, d\varepsilon = \sigma_{\beta}(T)\, \varepsilon_{\beta}^{tr}(T)$$

is the energy generated per unit volume in translating a single β-domain wall. Therefore, the total energy per unit volume is

$$\mathcal{E}(T) = \sum_{\beta} E_{\beta}(T). \tag{23}$$

We reformulate (23) as

$$\mathcal{E}(T) = \bar{\sigma}(T) \sum_{\beta} \varepsilon_{\beta}^{tr}(T) \tag{24}$$

where

$$\bar{\sigma}(T) = \frac{\sum_{\beta} \sigma_{\beta}(T)\, \varepsilon_{\beta}^{tr}(T)}{\sum_{\beta} \varepsilon_{\beta}^{tr}(T)}. \tag{25}$$

Following Jiles and Atherton, we assume that the energy required to move a domain wall across a pinning site is proportional to the energy of unimpeded domain wall movement. Letting n_{β} denote the number density of pinning sites at a β-domain wall, we approximate the pinning energy density by

$$\mathcal{E}_{pin}(T) = C\bar{\sigma}(T) \sum_{\beta} n_{\beta} \varepsilon_{\beta}^{tr}(T), \tag{26}$$

where C is a proportionality factor. One can establish a constant C in terms of quantities at a fixed temperature. For $T = T_c$, (26) simplifies to

$$\mathcal{E}_{pin}(T_c) = C\sigma_{\mp}(T_c)\, n_{\mp} \varepsilon_{\mp}^{tr}(T_c). \tag{27}$$

It follows that,

$$C = \frac{\mathcal{E}_{pin}\left(T_c\right)}{\sigma_{\mp}\left(T_c\right) n_{\mp}\varepsilon_{\mp}^{tr}\left(T_c\right)}, \tag{28}$$

so that (26) becomes

$$\mathcal{E}_{pin}\left(T\right) = \frac{\mathcal{E}_{pin}\left(T_c\right)\bar{\sigma}\left(T\right)}{\sigma_{\mp}\left(T_c\right) n_{\mp}\varepsilon_{\mp}^{tr}\left(T_c\right)} \sum_{\beta} n_{\beta}\varepsilon_{\beta}^{tr}\left(T\right). \tag{29}$$

We assume the $\bar{\sigma}\left(T\right)$ varies little over practical temperature ranges, hence we approximate $C\bar{\sigma}\left(T\right)$ by a constant k. We also recognize that the total change in strain accompanying pinned wall translation in an elemental volume is

$$d\varepsilon_{ir} = \sum_{\beta} n_{\beta}\varepsilon_{\beta}^{tr}\left(T\right).$$

Finally, we take as the total averaged pinning energy density

$$E_{pin}\left(\varepsilon_{ir}\right) = k\int_V d\varepsilon_{ir}, \tag{30}$$

where integration is over macroscopic volume V. To account for the shearing of a distribution of grain orientations, we employ techniques used in Section 2.2, which results in a re-scaled value of k. Accordingly, we treat the pinning parameter as an effective macroscopic quantity, which we must fit to experimental data.

3.2 Effective Stress

Material inhomogeneities, lattice defects, and polycrystalline structure give rise to local stress variations which yield self-stressed domains and variations in local critical temperatures [16]. To account for these variations in the bulk material, we use an interaction field relation described in [21, 27] for structural phase transitions. The total loading of a crystal element is the effective stress σ_e, which incorporates both the applied stress and an internal stress field coupled to the overall deformation

$$\sigma_e = \sigma - \alpha\varepsilon. \tag{31}$$

The mean-field constant α represents the average variation in the stress field. The nonlinear stress-strain law incorporating σ_e is

$$\sum_{j=3}^{m} a_{2j}\varepsilon_{an}^{2j-1} - a_4\varepsilon_{an}^{3} + a_2\left(T - T_c\right)\varepsilon_{an} = \sigma_e, \tag{32}$$

subject to (22). For the case $\varepsilon \approx \varepsilon_{an}$, the direct effect of α in (32) is that the phase transition at T_c, which would occur without mean-field effects, occurs at an effective temperature $T_c^e = T_c - \alpha/a_2$. In general, the effective energy coefficients, α and T_c are macroscopic quantities that represent statistical averages of microscopic phenomena. In Section 4.1, we discuss their identification. We note that (31) is analogous to the mean-field relations used in [33, 56] for magnetic and ferroelectric compounds and the one introduced in [66] for LiCsSO$_4$ crystals. Along with pinning, effective stresses significantly affect the motion of phase boundaries, which we treat next.

3.3 Irreversible Strain

Motivated by the Jiles-Atherton framework, we characterize the strain comprised of domain wall translations by establishing an energy balance in terms of ε_{ir}. The elastic work performed by an effective stress on the material is

$$E = \int \sigma_e (\varepsilon) \, d\varepsilon. \tag{33}$$

In our formulation of the model where strains are the response to applied stresses, it will be more convenient quantify work in terms of the complementary energy

$$\int_0^{\sigma_e} \varepsilon (\tilde{\sigma}_e) \, d\tilde{\sigma}_e = \sigma_e \varepsilon - \int_0^{\varepsilon} \sigma_e (\tilde{\varepsilon}) \, d\tilde{\varepsilon}, \tag{34}$$

for all $\sigma_e (\varepsilon)$ and $\varepsilon (\sigma_e)$ that are monotone increasing. It follows that the energy expended in moving domain walls across defects is the corresponding equilibrium elastic energy reduced by the energy dissipated due to pinning

$$\int_V \varepsilon_{ir} (\sigma_e) \, d\sigma_e = \int_V \varepsilon_{an} (\sigma_e) \, d\sigma_e - k \int_V \left(\frac{d\varepsilon_{ir}}{d\sigma_e} \right) d\sigma_e. \tag{35}$$

In (35), the last term is derived from (30) and the effective stress is defined in (31). The associated equation of state with respect to the effective stress is

$$\varepsilon_{ir} = \varepsilon_{an} - \delta k \frac{d\varepsilon_{ir}}{d\sigma_e}, \tag{36}$$

where δ is a directional parameter that ensures that pinning opposes changes in the effective stress

$$\delta = \begin{cases} +1 \text{ increasing } \sigma_e \\ -1 \text{ decreasing } \sigma_e. \end{cases}$$

Then (36) reduces to

$$\varepsilon_{an} - \varepsilon_{ir} = \delta k \frac{d\varepsilon_{ir}}{d\sigma} \left(\frac{1}{1 - \alpha \frac{d\varepsilon}{d\sigma}} \right) \tag{37}$$

in terms of the applied stress σ. Therefore, there is a coupling between the dynamics of the irreversible and total strains

$$\frac{d\varepsilon_{ir}}{d\sigma} = \frac{\varepsilon_{an} - \varepsilon_{ir}}{\delta k} \left(1 - \alpha \frac{d\varepsilon}{d\sigma} \right). \tag{38}$$

Once we derive an expression for the reversible strain in the next section, we shall use (38) to obtain an ODE solely in terms of the total and equilibrium strains. Alternatively, effective fields in [33, 56] employ a coupling with the *irreversible* quantity, which implies $\sigma_e = \sigma - \alpha \varepsilon_{ir}$ in (36). This is a viable approximation if changes of the reversible strains in the material are relatively small so that

$$\frac{d\varepsilon}{d\sigma} \approx \frac{d\varepsilon_{ir}}{d\sigma}.$$

In this case (37) yields a decoupled nonlinear ODE for ε_{ir}

$$\frac{d\varepsilon_{ir}}{d\sigma} = \frac{\varepsilon_{an} (\sigma_e) - \varepsilon_{ir} (\sigma)}{\delta k + \alpha \left[\varepsilon_{an} (\sigma_e) - \varepsilon_{ir} (\sigma) \right]}. \tag{39}$$

This form of the model is directly analogous to the irreversible magnetization and polarization models in [33, 56]. In effect, (39) quantifies the motion of phase boundaries across inclusions, relative to their ideal motion in the absence of inclusions. To describe domain wall motion in ferroelastics, which is manifested by structural interactions dominated by reversible elastic effects, we consider the form in (38). The quantification of reversible strains completes our characterization of the measured strain.

3.4 Reversible Strain

We define reversible strain ε_{re} to be the macroscopic strain brought about by domain wall bending in the presence of pinning mechanisms. Particularly, we take domain wall bending in ferroelastics to be domain wall movement that is not associated with structural phase transitions responsible for wall translation. Then, for ferroelastics we assume that the energy involved in reversible domain motion is a fraction of the difference in the ideal and irreversible energies

$$\int_V \varepsilon_{re}\left(\sigma_e\right) d\sigma_e = c_{re}\left(\int_V \varepsilon_{an}\left(\sigma_e\right) d\sigma_e - \int_V \varepsilon_{ir}\left(\sigma_e\right) d\sigma_e\right), \tag{40}$$

where $c_{re} \in [0,1]$ represents the unitless reversibility coefficient. Therefore, the reversible strain can be formulated as

$$\varepsilon_{re} = c_{re}\left(\varepsilon_{an} - \varepsilon_{ir}\right). \tag{41}$$

In the analogous models for ferromagnetics and ferroelectrics, where domain wall bending is characterized by planar walls bulging spherically about pinning sites, [33, 34, 38, 56] similarly argue that reversible quantities reduce the difference of the irreversible and anhysteretic phenomena. We treat c_{re} as a measure of the flexibility of ferroelastic domain walls as in [33], and estimate c_{re} for a particular ferroelastic compound through data fits. For the ferromagnetic and ferroelectric cases, it is related to the domain wall surface energy, the domain magnetization or polarization, and the average spacing between localized pinning sites.

3.5 Total Strain

The combination of the irreversible and reversible strain yields the total measured strain

$$\begin{aligned} \varepsilon &= \varepsilon_{ir} + \varepsilon_{re} \\ &= \left(1 - c_{re}\right)\varepsilon_{ir} + c_{re}\varepsilon_{an}. \end{aligned} \tag{42}$$

As described in [49], ferroelastic domains and domain walls move to minimize the elastic energy in the crystal. For a given applied stress, the anhysteretic strain represents a minimum energy configuration as discussed in the previous section and analogously in [34, 38]. Therefore, if a depinned domain wall achieves its equilibrium configuration, we expect translation to virtually cease, and so the observed bulk strain ε will be dominated by ε_{re}. Based on this idea and similar analysis in [38, 56], we derive the following relation from (42).

$$\frac{d\varepsilon}{d\sigma} = \left(1 - c_{re}\right)\tilde{\delta}\frac{d\varepsilon_{ir}}{d\sigma} + c_{re}\frac{d\varepsilon_{an}}{d\sigma},$$

where $\tilde{\delta} = 1$ for all points (σ, ε) that lie outside the anhysteretic region bounded by the equilibrium curves and $\tilde{\delta} = 0$ otherwise. From (32) we have

$$\frac{d\varepsilon_{an}}{d\sigma} = \left(1 - \alpha\frac{d\varepsilon}{d\sigma}\right) P\left(\varepsilon_{an}\right)^{-1} \tag{43}$$

where

$$P\left(\varepsilon_{an}\right)=\sum_{j=3}^{m}\left(2j-1\right)a_{2j}\varepsilon_{an}^{2j-2}-3a_4\varepsilon_{an}^{2}+a_2\left(T-T_c\right) \tag{44}$$

is equivalent to the left-hand side of (22), so $P\left(\varepsilon_{an}\right)>0$. Using (43) and the expression for ε_{ir} in (38) yields

$$\begin{aligned}\frac{d\varepsilon}{d\sigma}&=\left(1-c_{re}\right)\tilde{\delta}\frac{\varepsilon_{an}-\varepsilon_{ir}}{\delta k}\left(1-\alpha\frac{d\varepsilon}{d\sigma}\right)+c_{re}\left(1-\alpha\frac{d\varepsilon}{d\sigma}\right)P\left(\varepsilon_{an}\right)^{-1}\\&=\left(\tilde{\delta}\frac{\varepsilon_{an}-\varepsilon}{\delta k}+\frac{c_{re}}{P\left(\varepsilon_{an}\right)}\right)\left(1-\alpha\frac{d\varepsilon}{d\sigma}\right)\end{aligned}$$

since $\left(1-c_{re}\right)\left(\varepsilon_{an}-\varepsilon_{ir}\right)=\varepsilon_{an}-\varepsilon$. Therefore,

$$\frac{d\varepsilon}{d\sigma}=\frac{\tilde{\delta}\left(\varepsilon_{an}-\varepsilon\right)+\delta k c_{re}P\left(\varepsilon_{an}\right)^{-1}}{\delta k+\alpha\left[\tilde{\delta}\left(\varepsilon_{an}-\varepsilon\right)+\delta k c_{re}P\left(\varepsilon_{an}\right)^{-1}\right]}, \tag{45}$$

where $\varepsilon_{an}\left(\sigma_e\right)$ solves (32). Suitable initial conditions depend on the temperature T and initial stress; we take $\varepsilon(0)=0$ for nominal superelastic applications. We note that the case where $\tilde{\delta}=0$ simplifies to

$$\frac{d\varepsilon}{d\sigma}=\frac{c_{re}}{c_{re}\alpha+P\left(\varepsilon_{an}\right)},$$

which represents the reversible strain dynamics solely in terms of anhysteretic contributions. The first-order nonlinear differential equation (45) is the full domain model for ferroelastics. Table 1 summarizes the model parameters and their physical origin. In the next section, we illustrate solutions to the model and compare results to experimental superelastic data.

Parameter	**Physical Description**
T_c	Temperature below which a single domain of austenite is unstable.
k	Pinning constant; quantifies the energy dissipation due to material inclusions.
c_{re}	Reversibility coefficient; determines the contribution of reversible effects.
α	Mean-field constant; characterizes internal stresses manifested by material inhomogeneities.
a_{2j}, $j=1\cdots m$	Effective Gibbs free energy coefficients.
δ	Pinning switch that ensures that the friction-like pinning opposes loads.
$\tilde{\delta}$	Irreversibility switch that turns off irreversible effects when the equilibrium is reached.

Table 1: Description of model parameters.

4 Numerical Simulations and Validation

To numerically integrate the model, we employ a modified implicit Euler routine. In addition, we apply numerical scaling in solving the equilibrium equation (32) and in evaluating (44) to account for the typically large values of the nonlinear elastic constants and small strain values. Figure 5 illustrates model simulations at different fixed temperatures using three energy coefficients. As in Figure 4, we plot strain versus stress, treating deformation as the result of prescribed loads. The parameters values used are $T_c = 273\,\mathrm{K}$, $k = 10\,\mathrm{MJ}\,/\,\mathrm{m}^3$, $c_{re} = 0.50$, $\alpha = 7 \times 10^3\,\mathrm{MPa}$, $a_2 = 1.275 \times 10^3\,\mathrm{MPa}\,/\,\mathrm{K}$, $a_4 = 1.963 \times 10^7\,\mathrm{MPa}$, and $a_6 = 3.665 \times 10^9\,\mathrm{MPa}$.

The effective Gibbs free energy coefficients a_{2j} determine the shape of the non-transition regions, the temperature-dependent transformation points, and the size of the superelastic temperature interval. The transition temperature $T_c > 0$ shifts the temperature range where superelasticity occurs. The mean-field constant $\alpha \geq 0$ controls the slope of the transition regions, where small values yield abrupt transitions. The pinning parameter $k > 0$ controls the curvature of the transition regions, where large values round the end of transition lines and can prevent loop closure. Finally, the reversibility coefficient $c_{re} \in [0, 1]$ controls the curvature of the reversal paths with values close to zero yielding flat curves. In the following sections, we identify physical values for the model parameters and compare model simulations to experimental hysteresis data.

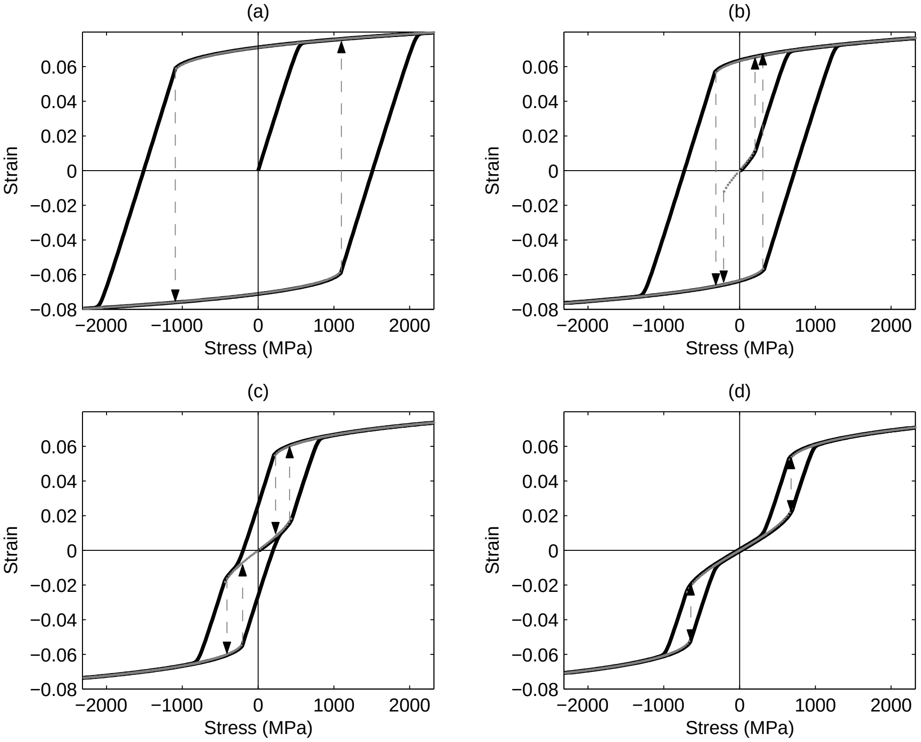

Figure 5: The domain model for temperatures (a) $T = 272\,\mathrm{K}$, (b) $T = 283\,\mathrm{K}$, (c) $T = 291\,\mathrm{K}$, and (d) $T = 298\,\mathrm{K}$. The gray segments and arrows correspond to the equilibrium strains calculated from (32).

4.1 Parameter Identification

Table 2 summarizes properties of the data used to characterize the domain model. The transformation temperatures are typically obtained from differential scanning calorimetry (DSC) or temperature-controlled resistivity measurements. We measure the slope S (in stress units) and width ε_T (i.e., transformation strain) using a single bounding hysteresis loop at fixed temperature T. For an initial iterate in a least-squares fitting routine, we calculate parameter estimates as follows. The bulk transition temperature T_c^e, which incorporates mean-field effects, is the average of M_s and M_f. A fit of the equilibrium stress-strain law (32) to the non-transition portions of the hysteresis loop yields the value $p_2 \equiv a_2(T - T_c) + \alpha$ and the higher-order energy coefficients $a_4, \cdots, a_{2m}$. It follows that

$$\hat{a}_2 = \frac{p_2}{T - T_c^e}. \tag{46}$$

is an estimate for a_2. The effective stress and pinning parameter estimates $\hat{\alpha}$ and $\hat{k}$ satisfy

$$\hat{\alpha} + \frac{2}{\varepsilon_T}\hat{k} = S. \tag{47}$$

Finally, we calculate the estimate $\hat{T}_c$ using the relation

$$\hat{T}_c = T_c^e + \frac{\hat{\alpha}}{p_2}\left(T - T_c^e\right). \tag{48}$$

Since the pinning constant is defined in terms of material properties that are not feasibly obtained, we determine a value of $\hat{k}$ according to initial simulations, and hence resolve (47) and (48). We refer the reader to [34] and [58] for parameter identification methods for the analogous ferromagnetic and ferroelectric models.

4.2 Model Validation

We compare our model with data from single-crystal and polycrystalline NiTi stress-strain experiments. In each case, we performed a fit to refine the parameter values obtained from properties of the data.

The single-crystal data from [26] corresponds to tensile experiments on NiTi of 50.8at.% Ti composition with a [211] orientation. To minimize the effects of material aging, a stabilized hysteresis loop was obtained after 16 cycles at 295 K. The measured transformation temperatures $M_s = 231\,\mathrm{K}$ and $M_f = 214\,\mathrm{K}$, and, with $S = 4457\,\mathrm{MPa}$ and $\varepsilon_T = 0.02$, we take $\hat{k} = 20\,\mathrm{MJ}\,/\,\mathrm{m}^3$ to obtain initial estimates of the remaining model parameters. Figure 6a illustrates the results for $m = 3, 5$. The parameter values resulting from the least-squares fitting routine for the $m = 5$ case are summarized in Table 3 and corresponding model predictions are compared with single crystal data in Figure 7a.

Measured Quantity	**Description**
M_s, M_f	Martensite start/finish temperatures.
S	Slope of transition regions.
ε_T	Strain-width of the transition region.

Table 2: Measured quantities used to estimate the model parameters.

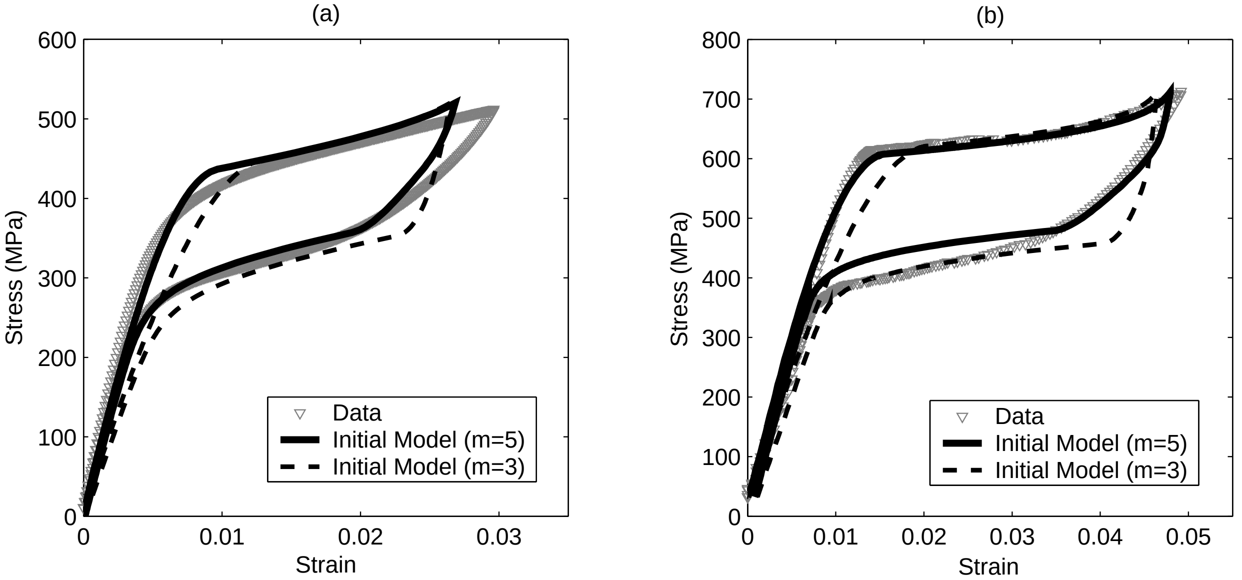

Figure 6: (a) Data from [26] for single-crystal NiTi, and (b) polycrystalline NiTi data from [9]. Each were measured at room temperature (295 K). Model simulations for three and five energy coefficients use initial parameter estimates obtained from the measured quantities in Table 2.

The polycrystalline data from [9] corresponds to tensile experiments on a polycrystalline NiTi wire of 55.0at.% Ti composition. The stabilized hysteresis loop was measured after a mechanical aging treatment of 22 cycles at 295 K. Subsequent minor loops were achieved by partial loading and complete unloading cycles. DSC measurements indicate the transformation temperatures $M_s = 302\,\mathrm{K}$ and $M_f = 273\,\mathrm{K}$. From the bounding loop, we measured $S = 1845\,\mathrm{MPa}$ and $\varepsilon_T = 0.035$, and from initial simulations we take $\hat{k} = 20\,\mathrm{MJ}\,/\,\mathrm{m}^3$. Figure 6b shows the simulations of the bounding loop using the initial parameter estimates. After fitting the $m = 5$ case, we simulated the hysteresis with cylces in Figure 7b. The associated parameter values are summarized in Table 3.

Data Set	Single-crystal	Polycrystal
T_c (K)	225	288
k (MJ / m^3)	13.31	20.39
c_{re}	0.95	0.90
α (MPa)	2457	698.8
a_2 (MPa / K)	9.358×10^2	8.430×10^3
a_4	3.195×10^8	1.059×10^8
a_6	7.395×10^{11}	8.775×10^{10}
a_8	-7.665×10^{14}	-3.224×10^{13}
a_{10}	2.987×10^{17}	4.465×10^{15}

Table 3: Parameter values used for model predictions in Figure 7. Coefficients a_4, a_6, a_8, and a_{10} have units of MPa .

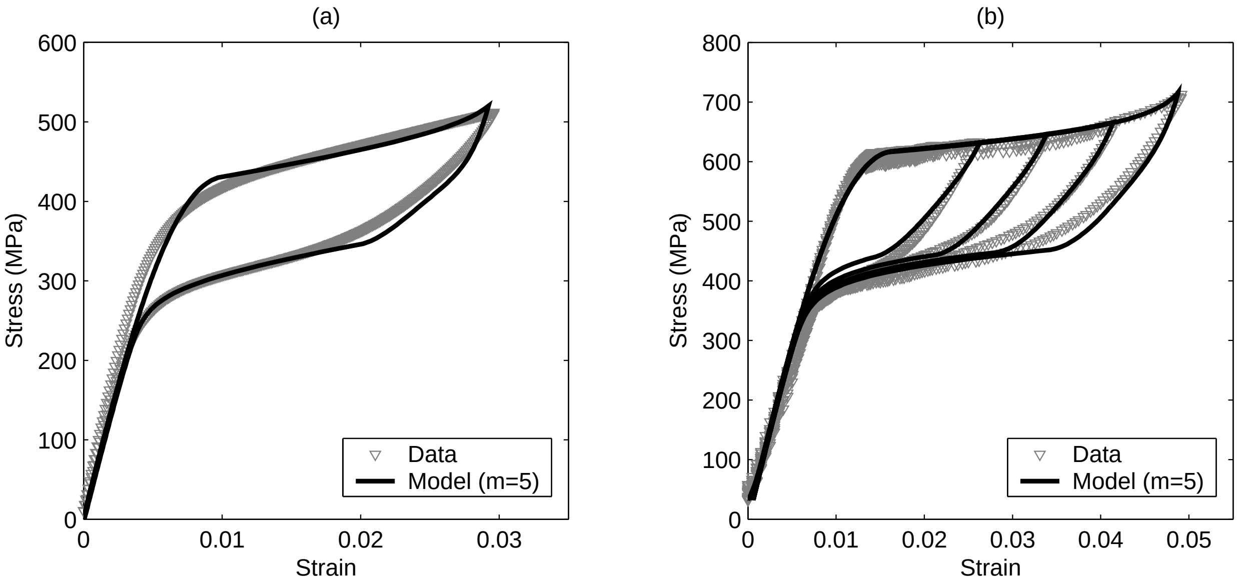

Figure 7: Hysteresis of (a) single-crystal NiTi data from [26], and (b) polycrystalline NiTi data from [9] measured at room temperature (295 K). Model predictions ($m = 5$) with parameters refined through least squares fit.

5 Concluding Remarks

In this paper, we have developed a model for temperature-dependent hysteresis in ferroelastics, with an emphasis on SMAs. The model predicts observed isothermal responses by modeling the evolution of ferroelastic domains under applied stresses. First, we use the Landau theory of phase transitions at the crystallographic level to derive effective equilibrium stress-strain equations at the macroscopic level. Then, considering the bending and translation of domain walls pinned at material inclusions, we account for energy losses associated with the propagation of phase boundaries. The resulting rate-independent model is analogous to the domain wall models developed in [33] for ferromagnetics, in [56] for ferroelectrics, and introduced in [66] for ferroelastic LiCsSO_4.

Altogether, our model requires $m + 4$ $(m \geq 3$ odd) material-dependent, effective parameters that we identify through measurements and least-squares fits to data. We show that with five effective energy coefficients ($m = 5$), the model provides excellent agreement with single-crystal and polycrystalline data experimental data. Moreover, our model is based on a single first order, nonlinear ordinary differential equation, which we solve numerically employing a simple modified implicit-Euler scheme. The simplicity of our model facilitates real-time parameter updating should it be required due to changing operating conditions. In addition, the low-order formulation makes it viable for incorporation into engineering design applications and for real-time implementation in model-based controllers. In particular, inverse compensator control methods have been used with ferromagnetic domain wall models [55].

As presented here, the model is rate-independent. While some applications may operate in quasi-static regimes that minimize rate effects, as noted in [54], internal SMA temperatures can change up to 10°C during loading cycles, even at moderate strain-rates in relatively isothermal environments. In addition, while the current equilibrium stress-strain equations (32) can approximate strain-temperature hysteresis, the shape memory effect, and latent heats of transformation [16], the full domain wall model cannot readily predict these phenomena particular to SMAs. To accommodate general ferroelastic and SMA behavior in more practical operating conditions, we intend to investigate these issues. Finally, we note that issues related to material aging are significant for a number of applications, but these are beyond the intent and scope of the model. To account for aging in real-time, the model parameters can be re-identified or adaptively updated if substantial discrepancies are detected.

Acknowledgments

The authors would like to thank Dr. Borut Bundara at ETRA 33 in Ljubljana, Slovenija and Dr. Ken Gall from the Department of Mechanical Engineering at the University of Colorado-Boulder for providing and supplementing the SMA hysteresis data used in this paper. This research was supported in part by the National Science Foundation under the grant CMS-0099764 and by the Air Force Office of Scientific Research through grant AFOSR-F49620-01-1-0107.

References

[1] R. Abeyaratne, K. Bhattacharya and J.K. Knowles, "Strain-energy functions with multiple local minima: modeling phase transformations using finite thermoelasticity," *Nonlinear Elasticity: Theory and Applications*, pp. 433-490 (Ch. 12), Cambridge University Press, 2001.

[2] G.R. Barsch, "Landau theory of structural transformations in titanium-nickel and gold-cadmium alloys," *Materials Science and Engineering: A*, Vols. 273-275, pp. 161-165, 1999.

[3] G.R. Barsch, "Landau theory of the displacive phase transformations in gold-cadmium and titanium-nickel alloys," *Materials Science Forum*, Vols. 327-328, pp. 367-376, 2000.

[4] D. Bernardini, "On the macroscopic free energy functions for shape memory alloys," *Journal of the Mechanics and Physics of Solids*, **49**(4), pp. 813-837, 2001.

[5] K. Bhattacharya and R.V. Kohn, "Symmetry, texture and the recoverable strain of shape-memory polycrystals," *Acta Materialia*, **44**(2), pp. 529-542, 1996.

[6] L.C. Brinson and M.S. Huang, "Simplifications and comparisons of shape memory alloy constitutive models," *Journal of Intelligent Material Systems and Structures*, Vol. 7, pp. 108-114, 1996.

[7] M. Brokate and J. Sprekels, *Hysteresis and Phase Transitions*, Applied Mathematical Sciences Volume 121, Springer, New York, NY, 1996.

[8] K. Brugger, "Thermodynamic definition of higher order elastic coefficients," *Physical Review B*, **133**(6A), pp. 1611-1612, 1964.

[9] B. Bundara, M. Tokuda, et. al., "Superelastic tension and bending characteristics of shape memory alloys," *Metals and Materials*, **6**(4), pp. 293-299, 2000.

[10] B. Bundara, "SMA: Present state and perspective for new applications," *Materials Science Forum*, Vols. 327-328, pp. 43-46, 2000.

[11] T. Castán, E. Vives and A. Planes, "Elastic constants of BCC binary alloys near the A_3B composition and their relation to martensitic transitions," *Journal of Physics: Condensed Matter*, **2**(7), pp. 1743-1752, 1990.

[12] D. Damjanovic, "Logarithmic frequency dependence of the piezoelectric effect due to pinning of ferroelectric-ferroelastic domain walls," *Physical Review B*, **55**(2), pp. R649-R652, 1997.

[13] R. DesRoches and M. Delemont, "Seismic retrofit of simply supported bridges using shape memory alloys," *Engineering Structures*, **24**(3), pp. 325-332, 2002.

[14] T. Duerig, A. Pelton and D. Stöckel, "An overview of nitinol medical applications," *Materials Science and Engineering: A*, Vols. 273-275, pp. 149-160, 1999.

[15] F. Falk, "Landau theory of martensitic phase transitions," *Journal de Physique Colloque*, **43**(C-4), pp. 3-15, 1982.

[16] F. Falk, "One-dimensional model of shape memory alloys," *Archives of Mechanics*, **35**(1), pp. 63-84, 1983.

[17] F. Falk, "Driven domain walls in shape memory alloys," *Journal of Physics C: Solid State Physics*, **20**(17), pp. 2501-2509, 1987.

[18] F. Falk, "Pseudoelastic stress-strain curves of polycrystalline shape memory alloys calculated from single crystal data," *International Journal of Engineering Science*, **27**(3), pp. 277-284, 1989.

[19] F. Falk and P. Konopka, "Three-dimensional Landau theory describing the martensitic phase transformation of shape-memory alloys," *Journal of Physics: Condensed Matter*, **2**(1), pp. 61-77, 1990.

[20] F. Falk, "Constitutive theories of shape memory alloys related to microstructure," *Proceedings of the SPIE*, Vol. 2442, pp. 2-10, 1995.

[21] M. Fujimoto, *The Physics of Structural Phase Transitions*, Springer-Verlag, New York, 1997.

[22] H. Funakubo, *Shape Memory Alloys*, translated from the Japanese by J.B. Kennedy, Gordon and Breach Science Publishers, Amsterdam, 1987.

[23] W.S. Galinaitis, D.S. Joseph and R.C. Rogers, "Parameter identification for Preisach models of hysteresis," *Proceedings of DETC'01 the ASME Design Engineering Technical Conference and Computers and Information in Engineering Conference*, Vol. 6, Pt. B, pp. 1409-1417, 2001.

[24] K. Gall and H. Sehitoglu, "The role of texture in tension-compression asymmetry in polycrystalline NiTi," *International Journal of Plasticity*, **15**(1), pp. 69-92, 1999.

[25] K. Gall, H. Sehitoglu and Y. Chumlakov, "NiTi experiments versus modeling: Where do we stand?" *Smart Structures and Materials 2000: Active Materials: Behavior and Mechanics, Proceedings of the SPIE*, Vol. 3992, pp. 536-547, 2000.

[26] K. Gall, H. Sehitoglu, et. al., "On the mechanical behavior of single crystal NiTi shape memory alloys and related polycrystalline phenomenon," *Materials Science and Engineering*, Vol. A317, pp. 85-92, 2001.

[27] J. Gonzalo, *Effective Field Approach to Phase Transitions and Some Applications to Ferroelectrics*, World Scientific, Singapore, 1991.

[28] C.W. Haas and W.F. Jaep, “Domain wall model for ferroelastics,” *Physics Letters A*, **49A**(1), pp. 77-78, 1974.

[29] D. Hughes and J.T. Wen, “Preisach modeling of piezoceramic and shape memory alloy hysteresis ,” *Smart Materials and Structures*, **6**(3), pp. 287-300, 1997.

[30] Y. Huo, “A mathematical model for the hysteresis in shape memory alloys,” *Continuum Mechanics and Thermodynamics*, **1**(4), pp. 283-303, 1989.

[31] A.P. Jardine, J. Bartley-Cho and J. Flanagan, “Improved design and performance of the SMA torque tube for the DARPA Smart Wing Program.” *Smart structures and materials 1999. Industrial and commercial applications of smart structures technologies.*, Vol. 3674, pp. 260-269, 1999.

[32] L. Jian and C.M. Wayman, “Compressive behavior and domain-related shape memory effect in $LaNbO_4$ ceramics,” *Materials Letters*, Vol. 26, pp. 1-7, 1996.

[33] D.C. Jiles and D.L. Atherton, “Theory of ferromagnetic hysteresis,” *Journal of Magnetism and Magnetic Materials,* **61**(1-2), pp. 48-60, 1986.

[34] D.C. Jiles, J.B. Thoelke and M.K. Devine, “Numerical determination of hysteresis parameters for the modeling of magnetic properties using the theory of ferromagnetic hysteresis,” *IEEE Transactions on Magnetics*, **28**(1), 1992.

[35] A. Ktena, D.I. Fotiadis, P.D. Spanos, et. al., “A Preisach model identification procedure and simulation of hysteresis in ferromagnets and shape-memory alloys,” *Physica B: Condensed Matter*, **306**(1-4), pp. 84-90, 2001.

[36] D.C. Lagoudas and A. Bhattacharyya, “On the correspondence between micromechanical models for isothermal pseudoelastic response of shape memory alloys and the Preisach model for hysteresis,” *Mathematics & Mechanics of Solids*, **2**(4), pp. 405-440, 1997.

[37] A.P. Levanyuk, “Interaction between ferroelastic domain walls mediated by thermal fluctuations and defects,” *Phase Transitions*, **B55**(1-4), pp. 127-133, 1995.

[38] F. Liorzou, B. Phelps and D.L. Atherton, “Macroscopic models of magnetization,” *IEEE Transactions on Magnetics*, **36**(2), 2000.

[39] J.E. Massad and R.C. Smith, “Domain wall model for SMA characterization,” *Smart structures and materials 2002: Modeling, Signal Processing, and Control, Proceedings of the SPIE*, Vol. 4693, pp. 324-335, 2002.

[40] Y. Matsuzaki, K. Funami and H. Naito, “Inner loops of pseudoelastic hysteresis of shape memory alloys: Preisach approach,” *Smart Structures and Materials 2002: Active Materials: Behavior and Mechanics, Proceedings of the SPIE*, Vol. 4699, pp. 355-364, 2002.

[41] V. Mueller, A. Fuith, J. Fousek, H. Warhanek and H. Beige, “Spontaneous strain in ferroelastic incommensurate $[N(CH_3)_4]_2CuCl_4$ crystals,” *Solid State Communications*, **104**(8), pp. 455-458, 1997.

[42] I. Müller and H. Xu, “On the pseudo-elastic hysteresis,” *Acta Metallurgica et Materialia*, **39**(3), pp. 263-271, 1991.

[43] R.E. Newnham, “Molecular mechanisms in smart materials,” *MRS Bulletin,* **22**(5), pp. 20-34, 1997.

[44] N. Papenfuss and S. Seelecke, “Simulation and control of SMA actuators,” *Smart structures and materials 1999: Mathematics and control in smart structures, Proceedings of the SPIE*, Vol. 3667, pp. 586-595, 1999.

[45] E. Patoor and M. Berveiller, “Micromechanical modeling of the thermomechanical behavior of shape memory alloys,” *Mechanics of Solids with Phase Changes*, pp. 121-188, 1997.

[46] A. Planes and L. Mãnosa, “Pretransitional effects in martensitic transitions,” *Materials Science Forum*, Vols. 327dvips -Ppdf -f file ¿ file.ps-328, pp. 421-428, 2000.

[47] H. Prahlad and I. Chopra, “Comparative evaluation of shape memory alloy constitutive models with experimental data,” *Journal of Intelligent Material Systems and Structures*, **12**(6), pp. 383-394, 2001.

[48] V. Prieb, T. Link, et. al., “Influence of the structure and orientation of the parent phase on the hysteresis of single-crystal shape memory alloys,” *Journal de Physique IV (Colloque)*, **5**(C8), Pt. 2, pp. 913-918, 1995.

[49] A.L. Roytburd, “Elastic domains and polydomain phases in solids,” *Phase Transitions*, **B45**(1), pp. 1-34, 1993.

[50] S. Saadat, M. Noori, et. al., “Using NiTi SMA tendons for vibration control of coastal structures,” *Smart Materials and Structures*, **10**(4), pp. 695-704, 2001.

[51] E.K.H. Salje, *Phase Transitions in ferroelastic and co-elastic crystals: an introduction for mineralogists, material scientists, and physicists*, Cambridge University Press, New York, 1993.

[52] E.K.H. Salje, “Ferroelasticity,” *Contemporary Physics*, **41**(2), pp. 79-91, 2000.

[53] B. Schroeder, C. Boller, et. al., “Comparative assessment of models for describing the constitutive behaviour of shape memory alloys,” *Smart materials and structures: proceedings of the 4th European Conference on Smart Structures and Materials in conjunction with the 2nd International Conference on Micromechanics, Intelligent Materials, and Robotics*, pp. 305–312, 1998.

[54] J.A. Shaw and S. Kyriakides, “Thermodynamic aspects of NiTi,” *Journal of the Mechanics and Physics of Solids*, **43**(8), pp. 1243-1281, 1995.

[55] R.C. Smith, “Inverse compensation for hysteresis in magnetostrictive transducers,” *Mathematical and Computer Modelling*, **33**(1-3), pp. 285-298, 2001.

[56] R.C. Smith and C.L. Hom, “Domain wall theory for ferroelectric hysteresis,” *Journal of Intelligent Material Systems and Structures*, **10**(3), pp. 195-213, 1999.

[57] R.C. Smith and J.E. Massad, “A Unified Methodology for Modeling Hysteresis in Ferroelectric, Ferromagnetic and Ferroelastic Materials,” *Proceedings of DETC’01 the ASME Design Engineering Technical Conference and Computers and Information in Engineering Conference*, Vol. 6, Pt. B, pp. 1389-1398, 2001.

[58] R.C. Smith and Z. Ounaies, “A domain wall model for hysteresis in piezoelectric materials,” *Journal of Intelligent Material Systems and Structures*, **11**(1), pp. 62-79, 2000.

[59] G. Sorge, H. Beige, et. al., “Elastic nonlinearity of $KH_3(SeO_3)_2$ and $KD_3(SeO_3)_2$ crystals,” *Physica Status Solidi A*, **73**(1), pp. K63-K66, 1982.

[60] G. Sorge, U. Straube and A. Almeida, “Investigations of ferroelastic phase transition by ultrasonic methods,” *Acta Physica Slovaca*, **32**(1), pp. 55-60, 1982.

[61] V. Stoilov and A. Bhattacharyya, “A theoretical framework of one-dimensional sharp phase fronts in shape memory alloys,” *Acta Materialia*, **50**(20), pp. 4939-4952, 2002.

[62] H. Tamai and Y. Kitagawa, “Pseudoelastic behavior of shape memory alloy wire and its application to seismic resistance member for building,” *Computational Materials Science*, **25**(1-2), pp. 218-227, 2002.

[63] J. Tolédano and P. Tolédano, “Order parameter symmetries and free-energy expansions for purely ferroelastic expansions,” *Physical Review B*, **21**(3), pp. 1139-1172, 1980.

[64] P. Tolédano, M. Fejer and B. Auld, “Nonlinear elasticity in proper ferroelastics,” *Physical Review B*, **27**(9), pp. 5717-5744, 1983.

[65] P. Tolédano and V. Dmitriev, *Reconstructive Phase Transitions*,World Scientific, New Jersey, 1996.

[66] J.A. Tuszyński, B. Mróz, et. al., “Comments on the hysteresis loop in ferroelastic $LiCsSO_4$,” *Ferroelectrics*, Vol. 77, pp. 111-120, 1988.

[67] D. Vanderbilt and H.C. Morrel, “Monoclinic and triclinic phases in higher-order Devonshire theory.”, *Physical Review B*, **63**(094108), pp. 1-9, 2001.

[68] A. Visitin, *Differential Models of Hysteresis*, Springer-Verlag, New York, 1994.

[69] G. Webb, A. Kurdila and D. Lagoudas, “Adaptive hysteresis model for model reference control with actuator hysteresis,” *Journal of Guidance, Control, and Dynamics*, **23**(3), pp. 459-465, 2000

[70] K. Wilde, P. Gardoni and Y. Fujino, “Base isolation system with shape memory alloy device for elevated highway bridges,” *Engineering Structures*, **23**(3), pp. 222-229, 2000.

[71] Y.Y. Ye, C.T. Chan and K.M. Ho, “Structural and electronic properties of the martensitic alloys TiNi, TiPd, and TiPt.”, *Physical Review B*, **56**(7), pp. 3678–3689, 1997.